

### Numerical Heat Transfer, Part B: Fundamentals



An International Journal of Computation and Methodology

ISSN: 1040-7790 (Print) 1521-0626 (Online) Journal homepage: http://www.tandfonline.com/loi/unhb20

# Fully implicit method for coupling multiblock meshes with nonmatching interface grids

M. Darwish, W. Geahchan & F. Moukalled

**To cite this article:** M. Darwish, W. Geahchan & F. Moukalled (2017) Fully implicit method for coupling multiblock meshes with nonmatching interface grids, Numerical Heat Transfer, Part B: Fundamentals, 71:2, 109-132, DOI: 10.1080/10407790.2016.1265299

To link to this article: <a href="http://dx.doi.org/10.1080/10407790.2016.1265299">http://dx.doi.org/10.1080/10407790.2016.1265299</a>

	Published online: 16 Feb 2017.
	Submit your article to this journal 🗷
ılıl	Article views: 80
Q <sup>L</sup>	View related articles 🗷
CrossMark	View Crossmark data 🗗
4	Citing articles: 2 View citing articles 🗷

Full Terms & Conditions of access and use can be found at http://www.tandfonline.com/action/journalInformation?journalCode=unhb20



## Fully implicit method for coupling multiblock meshes with nonmatching interface grids

M. Darwish, W. Geahchan, and F. Moukalled

Department of Mechanical Engineering, American University of Beirut, Beirut, Lebanon

#### **ABSTRACT**

A newly developed efficient and fully implicit method for multiblock mesh coupling that preserves the convergence characteristics of single-block meshing is presented. The technique is developed in the context of an unstructured pressure-based collocated finite-volume method, is applicable to both segregated and coupled flow solvers, and is ideal for code parallelization. The discretization at interfaces is performed in a separate step to stitch the regions sub-matrices into a global matrix. By solving the global matrix, the solution achieved to the multiregion problem is exactly the one that would result from a single-mesh discretization. The method is tested by solving three laminar flow problems. Solutions are obtained by meshing the domain as one block or by subdividing it into a number of blocks with non-matching grids at interfaces. Results show the very tight coupling at interfaces with a convergence rate that is independent of the number of blocks used.

#### ARTICLE HISTORY

Received 9 January 2016 Accepted 4 November 2016

#### Introduction

The efficiency of the numerical solution of the equations governing fluid flow is highly dependent on the quality and density of the mesh constructed to appropriately describe the geometry of interest and to resolve the physics involved. Too coarse mesh could lead the numerical solution to miss important features of the flow; while too dense mesh may cause the computational cost to become a hindrance. In addition, a highly skewed mesh causes numerical instabilities and negatively affects the quality of the solution [1–3]. These issues are of primary concern in domains with complex geometry and boundary conditions. Several techniques have been developed to address these problems. Error estimation [4, 5] is one technique used to guide the refinement of a coarse mesh. Another approach for reducing grid density is to use hybrid grids with anisotropic elements near boundaries and more isotropic elements in the core of the geometry.

When treating multiscale problems, i.e., problems where a large spectrum of time or length scales exist, finding an appropriate meshing strategy can become very difficult. In these problems, the grid spacing may be significantly different in different parts of the computational domain, often leading to unnecessary clustering of grid point through large parts of the domain [6, 7]. This is encountered when meshing complex geometries with large geometrical scales or when important flow features are present only in certain parts of the domain. In these cases, the resulting mesh system is either of poor quality or unnecessarily dense. Multiblock meshing, of interest in this paper, is one way to address this problem. In multiblock meshing, the domain is subdivided into blocks or regions that are meshed independently as appropriate. The regions are then reassembled and interconnected to recover the original computational domain.

#### Nomenclature coefficients in the discretized equations volume of element $b_C^{\phi}$ source term in the discretized φ equation Greek symbols B source term in the momentum equation scalar variable Cmain grid point dynamic viscosity μ $\mathbf{d}_{CF}$ vector joining the grid points C and F Γ diffusion coefficient $d_{CF}$ magnitude of $\mathbf{d}_{CF}$ fluid density ρ D operator used in the pressure equation deviatoric stress tensor τ $D_f^u, D_f^v$ components of the D operator $\partial V$ surface area of cell volume V component of the surface vector in the direction of $\mathbf{d}_{CF}$ Subscripts Е magnitude of E Cmain grid point F refers to neighbor of the C grid point f control volume face geometric interpolation factor g F F grid point I identity matrix пb values at the faces obtained by interpolation $J_f^{\text{Conv}}$ convection flux between C and its neighbors $J_f^{\text{Diff}}$ neighbors of the C grid point diffusion flux NBmass flow rate at control volume face f $\dot{m}_f$ Superscripts pressure p pressure S surface vector u-velocity component и $S_f^x$ , $S_f^y$ Components of the surface vector Sat v-velocity component ν element face f correction *u*, *v* velocity components in x- and y-direction, value at the previous iteration respectively interpolated value velocity vector

Multiblock regions can be assembled in such a way that the meshes overlap; the grid is then denoted as overlapping grid with a special class of this type denoted Chimera grid [8-10]. For this case, the inter-region interfaces are areas and volumes for two- and three-dimensional geometries, respectively. The blocks can also be assembled such that they fill the whole domain without any overlap; the grid is then denoted as abutting (nonoverlapping) grid. The inter-region interfaces become edges and areas in two- and three-dimensional domains, respectively. This work is restricted to abutting/nonoverlapping multiregion meshes.

One important issue in the treatment of multiregion meshes is resolving the information exchange at the inter-region interfaces, i.e., the interface coupling method. The interface coupling should ensure that (i) the solution obtained by decomposing the domain into several regions is exactly the one that would result from solving the problem as one block; (ii) the fluxes across the interfaces are fully conserved (i.e., the conserved flux variable leaving one region at an interface is equal to the flux entering the other region through the same interface); (iii) the accuracy of the discretization method is retained at the interfaces; (iv) the coupling technique is implemented efficiently with minimum overhead on memory and computational resources.

Interface coupling can be implemented either as an explicit [11–15] or an implicit [16, 17] iterative process. An explicit procedure involves two stages. In the first stage, a solution is sought for the different regions independently with the inter-region interfaces treated as boundary patches. In the second stage, the interfaces are updated using the newest region solutions by performing data exchange between the connected regions. The swap of information across regions is achieved by extrapolating data to the interface using the penalty methods [18], splines interpolation [19, 20] or other extrapolation techniques [21]. Again ensuring flux conservation across the interfaces is crucial. A major drawback of explicit methods is the convergence rate deterioration that occurs as the number of regions increases. This means that explicit coupling methods do not satisfy the efficiency criteria.

An implicit interface coupling method should ensure that the discretization of the various regions can be performed independently, while maintaining a strong implicit interface coupling to yield ideally a convergence rate that is independent of the number of connected regions.

The aim of this work is to present such an implicit coupling procedure that combines simplicity, conservativeness, and efficiency while retaining an optimal convergence rate that is similar to onegrid methods. The method is developed for arbitrary interface conditions on nonmatching grids within the context of a fully conservative, unstructured, pressure-based, segregated, and fully coupled finite volume flow solvers.

In the remainder of this article, the segregated and coupled solvers are briefly reviewed. This is followed by a detailed description of the interface coupling procedure. Finally, the performance of the newly developed procedure is demonstrated by presenting results to a set of problems with solutions obtained by decomposing the physical domain into several blocks and comparing results with the solution obtained when treating the physical domain as one block.

#### Discretization of the conservation equations in the finite volume method

The continuity and momentum equations for incompressible steady-state flow can be written as

$$\nabla \cdot (\rho \mathbf{v}) = 0 \tag{1}$$

$$\nabla \cdot (\rho \mathbf{v} \mathbf{v}) = -\nabla p - \nabla \cdot \mathbf{\tau} + \mathbf{B} \tag{2}$$

In the finite volume method, the domain is subdivided into several elements as shown in Figure 1(a). The discretization process starts by integrating the conservation equations over every element in the domain, such as the one shown in Figure 1(b), to yield

$$\int \int_{V} \nabla \cdot (\rho \mathbf{v}) \, \mathrm{d}V = 0 \tag{3}$$

$$\int \int_{V} \nabla \cdot (\rho \mathbf{v} \mathbf{v}) \, dV = -\int \int_{V} (\nabla \cdot pI) \, dV - \int \int_{V} (\nabla \cdot \tau) \, dV + \int \int_{V} \mathbf{B} \, dV \tag{4}$$

where the stress tensor is given by

$$\tau = -\mu \left( \nabla \mathbf{v} + \nabla \mathbf{v}^T - \frac{2}{3} (\nabla \cdot \mathbf{v}) \mathbf{I} \right)$$
 (5)

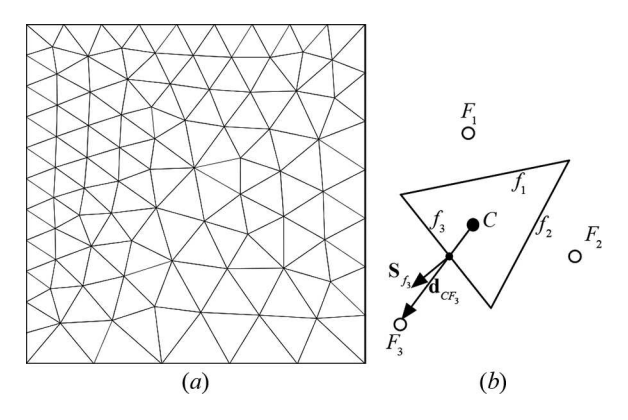


Figure 1. (a) A physical domain subdivided into several nonoverlaping triangular elements and (b) an element C with its attributes.

Green's theorem is used to transform the volume integrals of all fluxes and of the pressure gradient term into surface integrals, Eqs. (3) and (4) are transformed to

$$\oint_{\partial V} \rho \mathbf{v} \cdot d\mathbf{S} = 0$$
(6)

$$\oint_{\partial V} (\rho \mathbf{v} \mathbf{v}) \cdot d\mathbf{S} = -\oint_{\partial V} (p\mathbf{I}) \cdot d\mathbf{S} - \oint_{\partial V} \tau \cdot d\mathbf{S} + \int_{V} \mathbf{B} \, dV$$
 (7)

By evaluating the surface integrals over the discrete surfaces of the element shown in Figure 1(b), the discrete forms of the above equations become

$$\sum_{f=nb(C)} (\rho \mathbf{v} \cdot \mathbf{S})_f = 0 \tag{8}$$

$$\sum_{f=nb(C)} (\rho \mathbf{v} \mathbf{v} + \tau)_f \cdot \mathbf{S}_f + \sum_{f=nb(C)} (p_f \mathbf{I}) \cdot \mathbf{S}_f = \mathbf{B}_C V_C$$
(9)

In the momentum equation, the pressure at the control volume face f is linearly interpolated, using the values at the main grid points straddling the interface, as

$$p_f = g_f p_C + (1 - g_f) p_F (10)$$

#### The segregated finite volume flow solver

In a segregated flow solver [22–29], the pressure term appearing in the momentum equation [Eq. (9)] is moved to the right-hand side of the equation and treated explicitly. In addition, terms involving the  $\nu$ -velocity component appearing in the x-momentum equation, and vice versa, are also added to the source term and treated explicitly. Performing this step, the algebraic equations for the u- and  $\nu$ -velocity components are obtained as

$$a_{C}^{u}u_{C} + \sum_{F=NB(C)} a_{F}^{u}u_{F} = b_{C}^{u}$$

$$a_{C}^{v}v_{C} + \sum_{F=NB(C)} a_{F}^{v}v_{F} = b_{C}^{v}$$
(11)

Rather than solving for pressure directly, pressure is computed by transforming the continuity equation into a pressure correction equation. The derivation starts by defining correction fields for the velocity and pressure variables such that

$$u = u^* + u', v = v^* + v', p = p^* + p'$$
 (12)

where \* refers to values satisfying the momentum equations and ' to corrections needed to satisfy the continuity equation. Then, adopting the Rhie–Chow interpolation technique [30] that allowed the formulation of pressure-based algorithms on collocated grids [31–35], the velocity components at a control volume face in the continuity equation are written as

$$u_{f} = \overline{u_{f}} - \overline{D_{f}^{u}} \left( \nabla p_{f} - \overline{\nabla p_{f}} \right)$$

$$v_{f} = \overline{v_{f}} - \overline{D_{f}^{v}} \left( \nabla p_{f} - \overline{\nabla p_{f}} \right)$$
(13)



with correction values given by

$$u'_{f} = \overline{u'_{f}} - \overline{D_{f}^{u}} \left( \nabla p'_{f} - \overline{\nabla p'_{f}} \right)$$

$$v'_{f} = \overline{v'_{f}} - \overline{D_{f}^{v}} \left( \nabla p'_{f} - \overline{\nabla p'_{f}} \right)$$
(14)

Substituting in the continuity equation and adopting the Semi-Implicit Method for Pressure Linked Equations (SIMPLE) algorithm approximation [22-24, 27, 28, 31-35], the pressure correction equation is obtained as

$$a_C^{p'}p'_C + \sum_{F=NR(C)} a_F^{p'}p'_F = b_C^{p'}$$
(15)

The term  $b_C^{p'}$  in the pressure correction equation is given by

$$b_C^{p'} = -\sum_{f=nb(C)} \dot{m}_f \tag{16}$$

where  $\dot{m}_f$  represents the mass flow rate at a cell face.

In the SIMPLE algorithm, solutions are obtained by solving sequentially the u, v, and p' equations. Corrections to the velocity and pressure fields are applied after solving the p' equation. This sequence of events is repeated until a converged solution, satisfying both momentum and continuity equations, is reached.

#### The coupled finite volume flow solver

In a fully implicit velocity-pressure coupled approach [36-40], the continuity and momentum equations are solved simultaneously to obtain pressure and velocity fields that satisfy both momentum conservation and mass conservation. Rather than a pressure correction equation, a pressure equation is derived from the continuity equation. The discretization of the momentum and continuity equations in the coupled approach differs from the segregated approach in few details.

In the coupled approach, the algebraic forms of the *u*- and *v*-momentum equations are obtained by combining Eqs. (9) and (10). For example, the algebraic equation for the u-velocity component is obtained as

$$a_{C}^{uu}u_{C} + \underline{\underline{a_{C}^{uv}v_{C}}} + \underline{a_{C}^{up}p_{C}} + \sum_{F=NB(C)} a_{F}^{uu}u_{F} + \sum_{F=NB(C)} a_{F}^{uv}v_{F} + \sum_{F=NB(C)} a_{F}^{up}p_{F} = b_{C}^{u}$$
(17)

where

$$a_F^{up} = (1 - g_f) S_f^x$$

$$a_C^{up} = \sum_{f=nb(C)} g_f S_f^x$$

$$(18)$$

In Eq. (17), the underlined pressure term is due to the pressure gradient which is now discretized implicitly, while the double underlined term for the v-velocity component arises only at the boundary as a result of the treatment of the shear stress.

Similarly for the  $\nu$ -velocity component, the following equation is obtained:

$$a_{C}^{vv}v_{C} + \underline{a_{C}^{vu}u_{C}} + \underline{a_{C}^{vp}p_{C}} + \sum_{F=NB(C)} a_{F}^{vv}v_{F} + \sum_{F=NB(C)} a_{F}^{vu}u_{F} + \sum_{F=NB(C)} a_{F}^{vp}p_{F} = b_{C}^{v}$$
 (19)

In the continuity equation, the velocity at a control volume face is also interpolated with the Rhie-Chow interpolation method. Using the vector form of Eq. (13), the continuity equation is transformed to

$$\sum_{f=nb(C)} \rho_f \left[ \overline{\mathbf{v}_f} - \overline{\mathbf{D}_f} \left( \nabla p_f - \overline{\nabla p_f} \right) \right] \cdot \mathbf{S}_f = 0$$
 (20)

which upon expansion becomes

$$\sum_{f=nb(C)} \rho_f \left( -\overline{\mathbf{D}_f} \nabla p_f \right) \cdot \mathbf{S}_f + \sum_{f=nb(C)} \rho_f \overline{\mathbf{v}_f} \cdot \mathbf{S}_f = \sum_{f=nb(C)} \rho_f \left( -\overline{\mathbf{D}_f} \overline{\nabla p_f} \right) \cdot \mathbf{S}_f$$
 (21)

Noting that

$$\overline{\mathbf{v}_f} = g_f \mathbf{v}_C + (1 - g_f) \mathbf{v}_F \tag{22}$$

the algebraic form of the pressure equation can be written as

$$a_C^{pp}p_C + \underline{a_C^{pu}u_C + a_C^{pv}v_C} + \sum_{F = NB(C)} a_F^{pp}p_F + \sum_{F = NB(C)} a_F^{pu}u_F + \sum_{F = NB(C)} a_F^{pv}v_F = b_C^p$$
 (23)

where the coefficients in the underlined terms are given by

$$a_F^{pu} = (1 - g_f) S_f^x \quad a_F^{pv} = (1 - g_f) S_f^y$$

$$a_C^{pu} = \sum_{f=nb(C)} g_f S_f^x \quad a_C^{pv} = \sum_{f=nb(C)} g_f S_f^y$$
(24)

In matrix form, the above set of algebraic continuity and momentum equations can be represented as

$$\begin{bmatrix} a_C^{uu} & a_C^{uv} & a_C^{up} \\ a_C^{vu} & a_C^{vv} & a_C^{pp} \\ a_C^{pu} & a_C^{pv} & a_C^{pp} \\ a_C^{pv} & a_C^{pv} & a_C^{pp} \\ \end{bmatrix} \begin{bmatrix} u_C \\ v_C \\ p_C \end{bmatrix} + \sum_{F=NB(C)} \begin{bmatrix} a_F^{uu} & a_F^{uv} & a_F^{up} \\ a_F^{vu} & a_F^{vv} & a_F^{pp} \\ a_F^{uu} & a_F^{vv} & a_F^{pp} \\ a_F^{uv} & a_F^{vv} & a_F^{pp} \\ \end{bmatrix} \begin{bmatrix} u_F \\ v_F \\ p_F \end{bmatrix} = \begin{bmatrix} b_C^{u} \\ b_C^{v} \\ b_C^{p} \\ \end{bmatrix}$$
(25)

A system of equations similar to Eq. (25) is obtained for each element in the computational domain and assembled into one system of equations. The system of equations is then iteratively solved until the set of equations converges to the final solution.

#### Implicit multiblock algorithm

The newly developed implicit multiblock algorithm is presented in this section and discussed by referring to the physical domain schematically depicted in Figure 2(a). As shown, the domain is decomposed into three blocks (blocks 1, 2, and 3) with each block meshed independently. As shown, blocks 1 and 3 and blocks 1 and 2 are interlinked at the interblock interfaces A and B, respectively. The discretization and solution of such system proceed in two stages: (i) an initialization phase that is performed at each time step to account for the case of moving blocks and (ii) a discretization stage that is performed during the coefficient loop iteration. In the initialization stage, all necessary topological data describing the connectivity at the interblock interfaces [e.g., A and B in Figure 2(a)] are derived including interblock face to element connections and contribution areas. The end result of this initialization step is the derivation of the interblock element connectivity [Figure 2(b)]. The topological data are then used during the interblock discretization stage, which starts after the discretization of the various blocks. In this stage, the block algebraic equations are stitched together into one algebraic system of equations [Figure 2(c)]. This is performed repeatedly for all equations forming the modeled physical system. The details of the operations performed in these two stages are presented below.

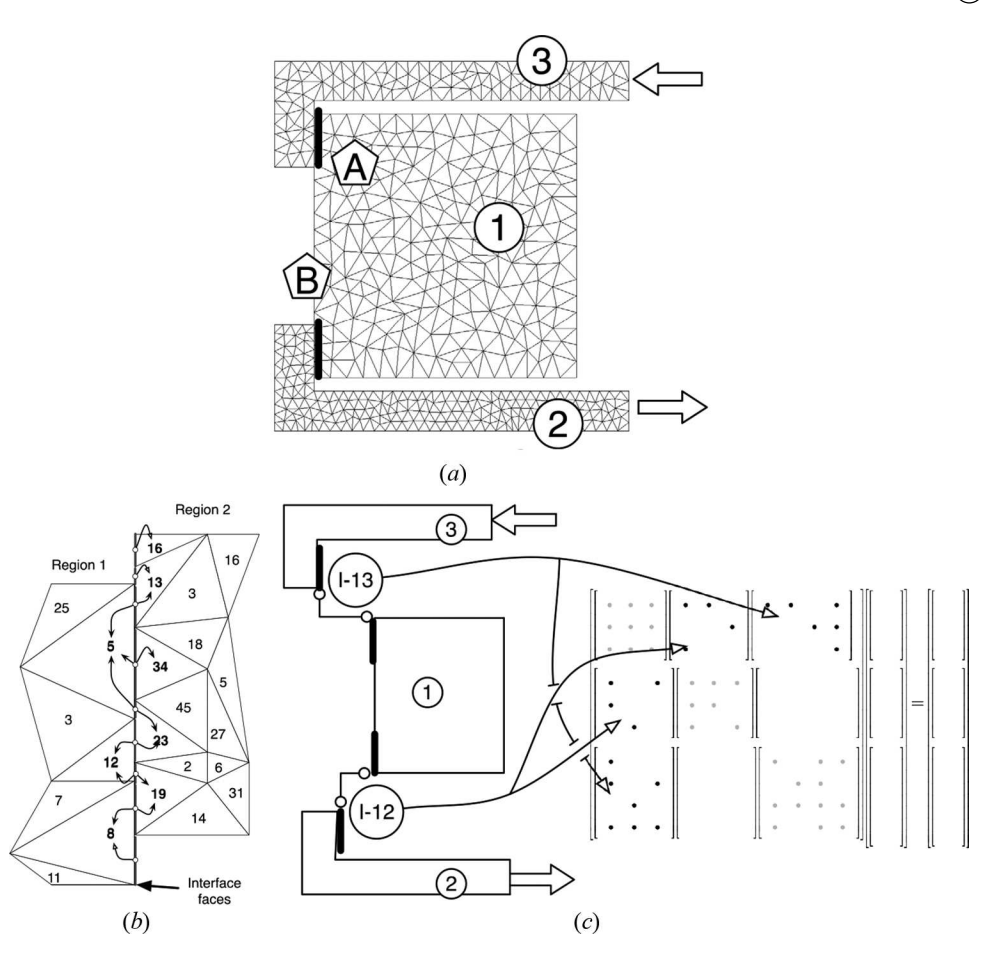


Figure 2. (a) A multiregion physical domain composed of regions 1, 2, and 3 that are independently meshed with interfaces between the different regions denoted by A and B, (b) topological data derived at the end of the initialization stage, and (c) stitching of algebraic equations into one system of equations accomplished at the end of the discretization stage.

#### Stage 1: Multiblock connectivity initialization

In the initialization stage, the interblock topological relations of the interface elements and faces of the connected regions are defined. This is to say that information on how the inter-region elements are connected and what is the strength of this connection, i.e., its relative area are computed. This step is performed at the start of each time step to allow for the moving of blocks (not considered in this work). The interface boundaries of the connected regions are first identified and the union of the interface regions is assigned a number of pixels [Figure 3(a)]. By defining the minimum number of pixels per face as a control parameter, the calculation of total number of pixels becomes straightforward. One pixel column is assigned at the interface for each of the two connected regions, with each pixel being associated with its parent element number [Figure 3(a)]. Using the two sets of pixel arrays, the topological and geometrical information of the interface faces can now be determined, based on the pair of elements associated with each position [Figure 3(b)].

A set of interface faces is then constructed using the pixel arrays described above. Each interface face extends over a length covered by identical pairs of numbered pixels [Figure 3(b)]. A pair of pixels is presented in the form (a, b) where "a" refers to the number associated with the pixel on the left pixel column while "b" refers to the number associated with the corresponding pixel on the right pixel column. For example, interface face 1 [Figure 3(b)] extends over a length covered by the pairs of

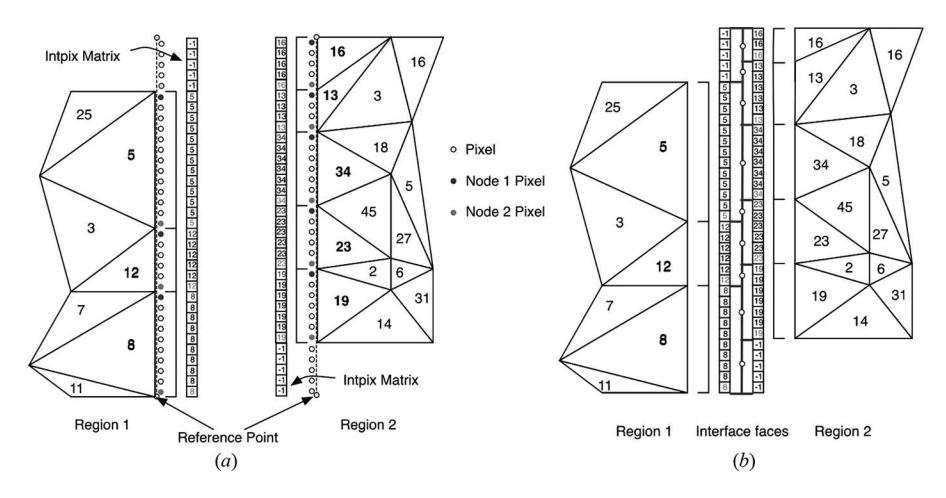
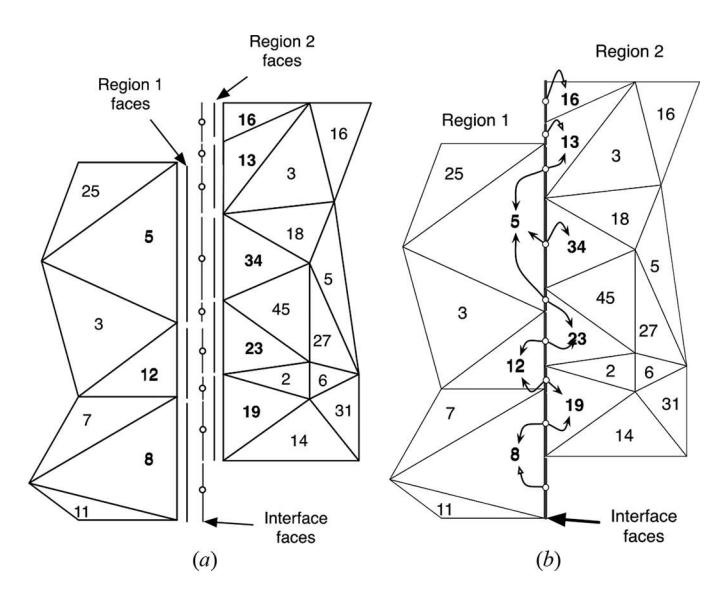


Figure 3. (a) Subdividing interface boundaries into pixels and (b) associating each pixel with its parent element number.

pixels (8, -1), interface face 2 extends over a length covered by the pairs of pixels (8, 19), and so on. An element face may be represented by one or more interface faces and may be connected to one or more cell faces from the opposite region. As shown in Figure 4(a), each interface face is also a part of one boundary face in each of the two regions. Topological information associated with these interface faces [Figure 4(b)] include: the local element indices to which the face links in each of the two regions, the area of the face (computed from the number of pixels forming the face), the face ratio of the interface face to the region boundary face, which will determine the contribution of the interface flux to the region boundary face. This is in addition to other secondary geometrical information that can be readily computed.

During discretization, a loop over the interface faces is performed to assemble the flux terms. These interface faces are used instead of the actual region boundary faces. The results are akin to having assembled one virtual mesh, with the obtained coefficients directly assembled into the global matrix of coefficients.



**Figure 4.** (a) Relation between interface faces and region boundary faces and (b) topological information associated with interface faces.

#### Stage 2: Interblock discretization

In the multiregion domain, the discretization of all flux terms is performed by looping, in all regions, over all interior and boundary faces that do not lie on an interblock patch and then by looping overall elements in the regions to calculate source and transient terms. This discretization stage yields a set of coefficients that are assembled together to form a local matrix of coefficients for each region [Figure 5(a)]. Then the local coefficient matrices are mapped into a global matrix through a simple reindexing scheme of the region elements as will be explained later.

After discretizing fluxes at interior and boundary faces, the flux terms at the interblock interface faces are discretized. The coefficients resulting from this discretization basically stitches or couples the various geometrically connected regions and are assembled into the global matrix of coefficients. As depicted in Figure 5(b), these coefficients fill the nondiagonal parts of the global matrix. During this discretization phase, the actual block interfaces are suppressed and the discretization is performed by looping overall interface faces. The discretization proceeds as in the case of internal faces, except that the interface faces connect elements from different regions and the terms are assembled directly into the global matrix.

The calculation of the mass, convection, and diffusion fluxes along interface faces is presented next by discretizing flux values along element face f, shown in Figure 6(a), that connects element C of region 1 to elements  $F_1$ ,  $F_2$ , and  $F_3$  of region 2 [Figure 6(b)].

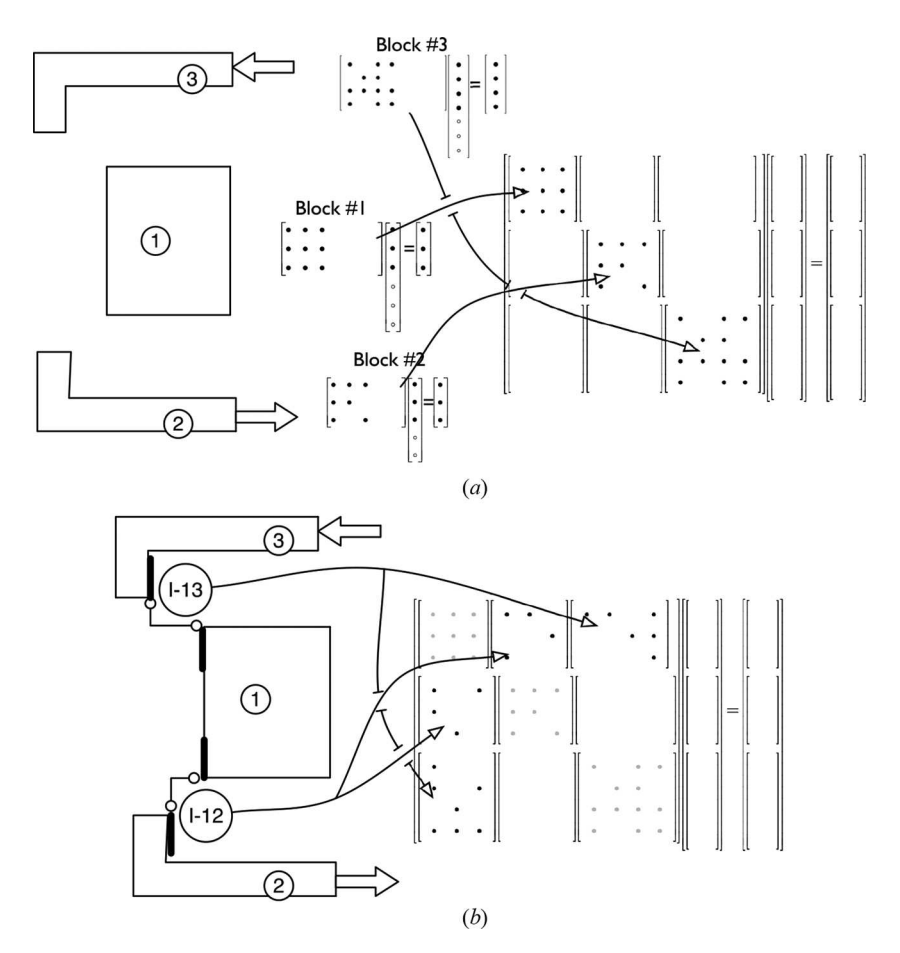


**Figure 5.** (a) Assembly of coefficients arising from the discretization of interior and boundary faces that do not belong to an interblock patch into local and global matrices (hollow circles are for interblock connections) and (b) assembly of coefficients arising from the discretization of interface faces into the global matrix.

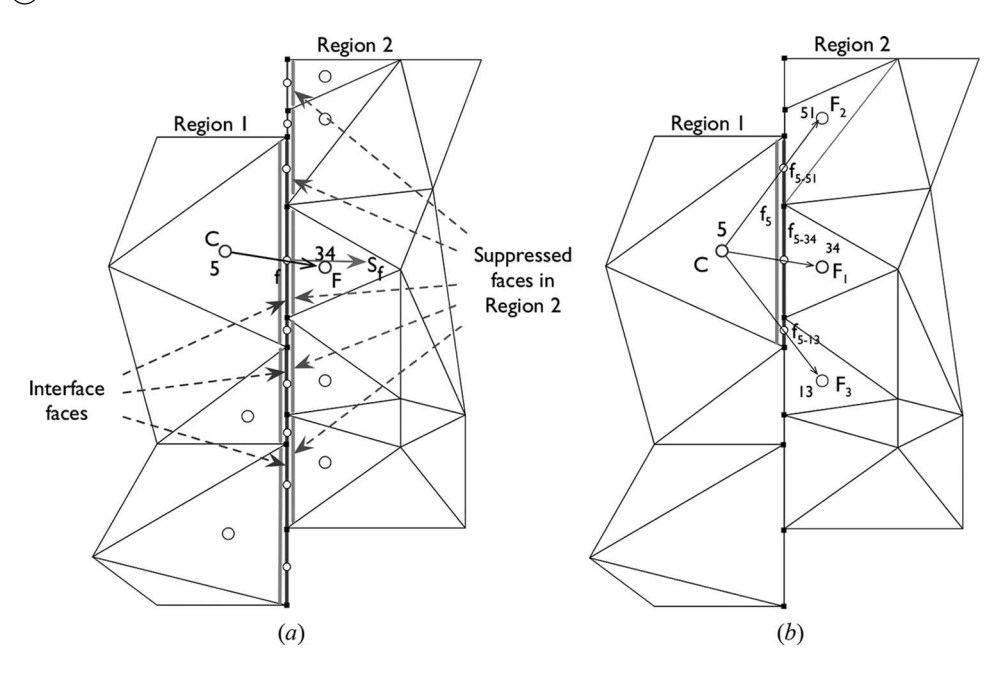


Figure 6. Discretization of fluxes along interface faces with (a) suppressed faces in region 2 and (b) notation used in deriving the algebraic relations.

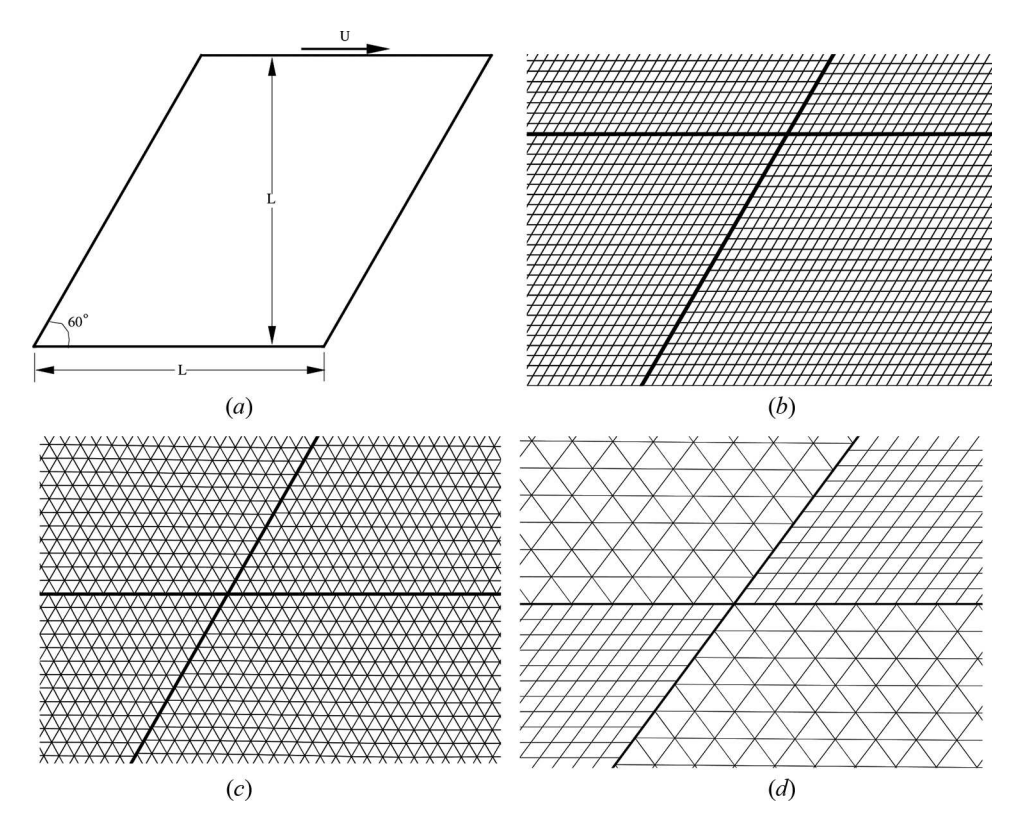


Figure 7. (a) Physical domain for the driven flow in a skew cavity problem; nonmatching grids at interfaces between blocks using (b) quadrilateral, (c) triangular, and (d) hybrid elements.

#### Discretization of the mass flux

The mass flux at the control volume face,  $f_5$ , which is needed to estimate the convective flux, is calculated as

$$\underbrace{\dot{m}_{f_{5}}}_{\text{control volume face}} = \underbrace{\dot{m}_{f_{5-34}} + \dot{m}_{f_{5-51}} + \dot{m}_{f_{5-13}}}_{\text{Interface faces}} = \rho_{f_{5-34}} \mathbf{v}_{f_{5-34}} \cdot \mathbf{S}_{f_{5-34}} + \rho_{f_{5-51}} \mathbf{v}_{f_{5-51}} \cdot \mathbf{S}_{f_{5-51}} + \rho_{f_{5-13}} \mathbf{v}_{f_{5-13}} \cdot \mathbf{S}_{f_{5-13}}$$

with face values computed using the Rhie-Chow formula.

For the continuity equation, the expressions for the mass fluxes differ depending on whether implementation is for the segregated or the coupled solver. For the segregated solver,  $\dot{m}_{f_s}$  is expressed as

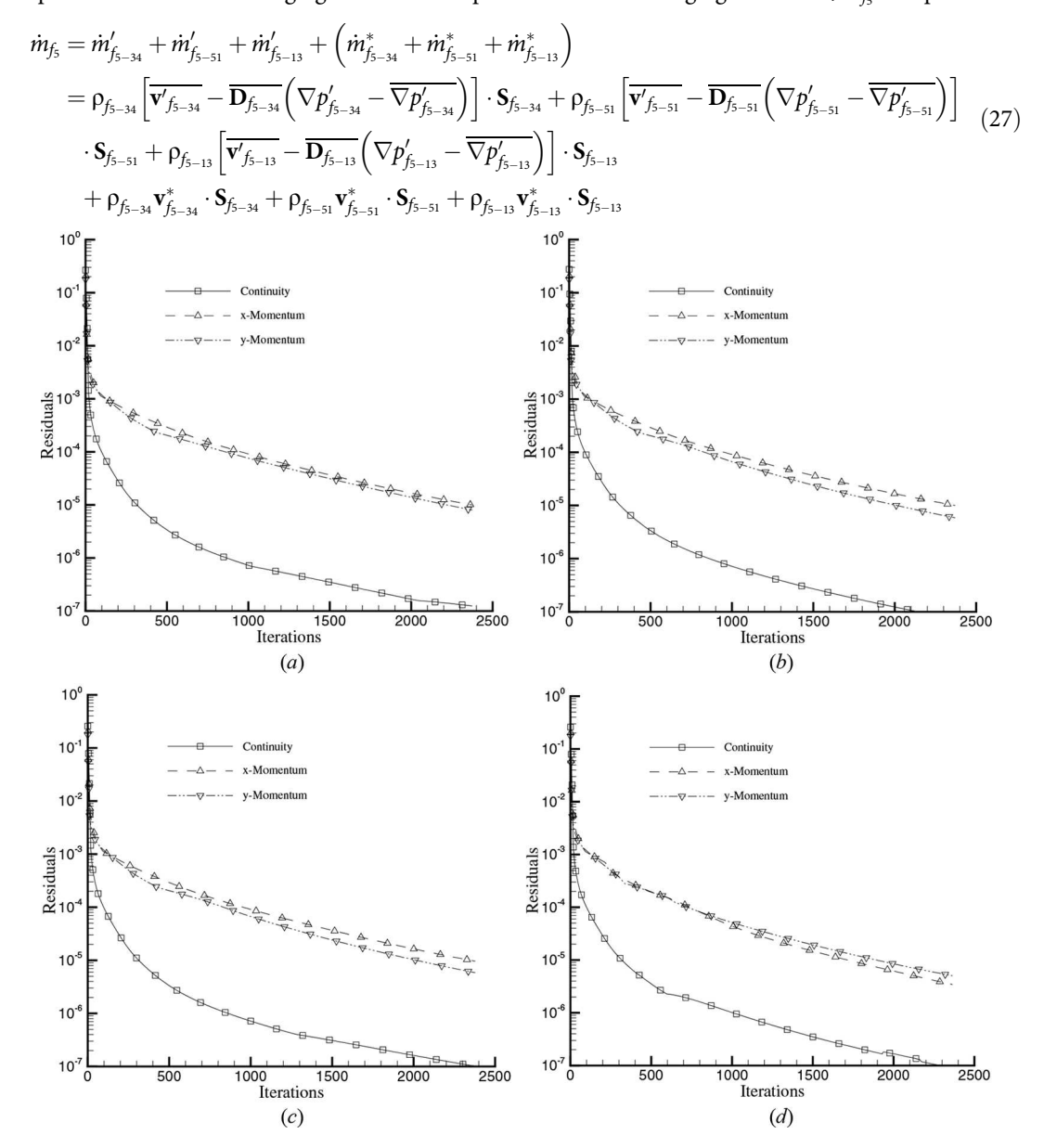


**Figure 8.** Reduction of residuals with iterations for the flow in a skew cavity using quadrilateral elements and the segregated flow solver with the domain subdivided into (a) one block, (b) two blocks, (c) four blocks, and (d) eight blocks.

Adopting the SIMPLE formulation, Eq. (27) is simplified to

$$\dot{m}_{f_{5}} = \dot{m}'_{f_{5-34}} + \dot{m}'_{f_{5-51}} + \dot{m}'_{f_{5-13}} + \left( \dot{m}^{*}_{f_{5-34}} + \dot{m}^{*}_{f_{5-51}} + \dot{m}^{*}_{f_{5-13}} \right) 
= -\rho_{f_{5-34}} \overline{\mathbf{D}_{f_{5-34}}} \nabla p'_{f_{5-34}} \cdot \mathbf{S}_{f_{5-34}} - \rho_{f_{5-51}} \overline{\mathbf{D}_{f_{5-51}}} \nabla p'_{f_{5-51}} \cdot \mathbf{S}_{f_{5-51}} - \rho_{f_{5-13}} \overline{\mathbf{D}_{f_{5-13}}} \nabla p'_{f_{5-13}} \cdot \mathbf{S}_{f_{5-13}} 
+ \rho_{f_{5-34}} \mathbf{v}^{*}_{f_{5-34}} \cdot \mathbf{S}_{f_{5-34}} + \rho_{f_{5-51}} \mathbf{v}^{*}_{f_{5-51}} \cdot \mathbf{S}_{f_{5-51}} + \rho_{f_{5-13}} \mathbf{v}^{*}_{f_{5-13}} \cdot \mathbf{S}_{f_{5-13}}.$$
(28)

In general, for an element i of region 1 connected to n elements of region 2, this equation is given by

$$\dot{m}_{f_i} = -\sum_{j=1}^n \rho_{f_{i-j}} \overline{\mathbf{D}_{f_{i-j}}} \nabla p'_{f_{i-j}} \cdot \mathbf{S}_{f_{i-j}} + \sum_{j=1}^n \rho_{f_{i-j}} \mathbf{v}^*_{f_{i-j}} \cdot \mathbf{S}_{f_{i-j}}$$
(29)

For the coupled solver, its expression becomes

$$\dot{m}_{f_{5}} = \rho_{f_{5-34}} \mathbf{v}_{f_{5-34}} \cdot \mathbf{S}_{f_{5-34}} + \rho_{f_{5-51}} \mathbf{v}_{f_{5-51}} \cdot \mathbf{S}_{f_{5-51}} + \rho_{f_{5-13}} \mathbf{v}_{f_{5-13}} \cdot \mathbf{S}_{f_{5-13}} 
= \rho_{f_{5-34}} \left[ \overline{\mathbf{v}_{f_{5-34}}} - \overline{\mathbf{D}_{f_{5-34}}} \left( \nabla p_{f_{5-34}} - \overline{\nabla p_{f_{5-34}}} \right) \right] \cdot \mathbf{S}_{f_{5-34}} + \rho_{f_{5-51}} \left[ \overline{\mathbf{v}_{f_{5-51}}} - \overline{\mathbf{D}_{f_{5-51}}} \left( \nabla p_{f_{5-51}} - \overline{\nabla p_{f_{5-51}}} \right) \right] \cdot \mathbf{S}_{f_{5-13}} 
+ \rho_{f_{5-13}} \left[ \overline{\mathbf{v}_{f_{5-13}}} - \overline{\mathbf{D}_{f_{5-13}}} \left( \nabla p_{f_{5-13}} - \overline{\nabla p_{f_{5-13}}} \right) \right] \cdot \mathbf{S}_{f_{5-13}}$$
(30)

Again the general expression of Eq. (30), for an element i of region 1 connected to n elements of region 2, is given by

$$\dot{m}_{f_i} = \sum_{i=1}^{n} \rho_{f_{i-j}} \left[ \overline{\mathbf{v}_{f_{i-j}}} - \overline{\mathbf{D}_{f_{i-j}}} \left( \nabla p_{f_{i-j}} - \overline{\nabla p_{f_{i-j}}} \right) \right] \cdot \mathbf{S}_{f_{i-j}}$$
(31)

Equations (29) and (31) are used in the derivation of the pressure correction equation and the pressure equation in the segregated and coupled solver, respectively.

**Table 1.** Comparison of the number of iterations required by the single-block and the multiblock meshing methods for the various problems solved using quadrilateral, triangular, and hybrid elements with the segregated and/or coupled solvers.

Number of blocks	Number of elements	Number of iterations
Driven flow in a skew cavity (quad	rilateral elements-segregated)	
1B	40,000	2,375
2B	39,998	2,372
4B	39,996	2,379
8B	39,992	2,365
Driven flow in a skew cavity (triand		
1B	104,796	23
2B	104,804	23
4B	104,614	23
8B	104,816	23
Driven flow in a skew cavity (hybri-	d elements-segregated)	
4B	31,402	2,174
Backward facing step (quadrilateral	elements-segregated)	,
1B	55,000	2,251
3B	55,000	2,244
Backward facing step (triangular ele	ements-segregated)	
1B	5,092	626
3B	5,026	632
Backward facing step (hybrid eleme	ents-segregated)	
3B	37,090	1,318
Sudden expansion in a square cavi	ty (quadrilateral elements-segregated)	
1B	48,000	1,909
6B	47.978	1,920
Sudden expansion in a square cavi	ty (triangular elements-segregated)	,
1B	26,970	2,304
6B	27,252	2,273
Sudden expansion in a square cavi	ty (hybrid elements-segregated)	,
6B	41,312	1,850



#### Discretization of the convection flux

Using the upwind scheme, the algebraic relation for the convection flux is written as

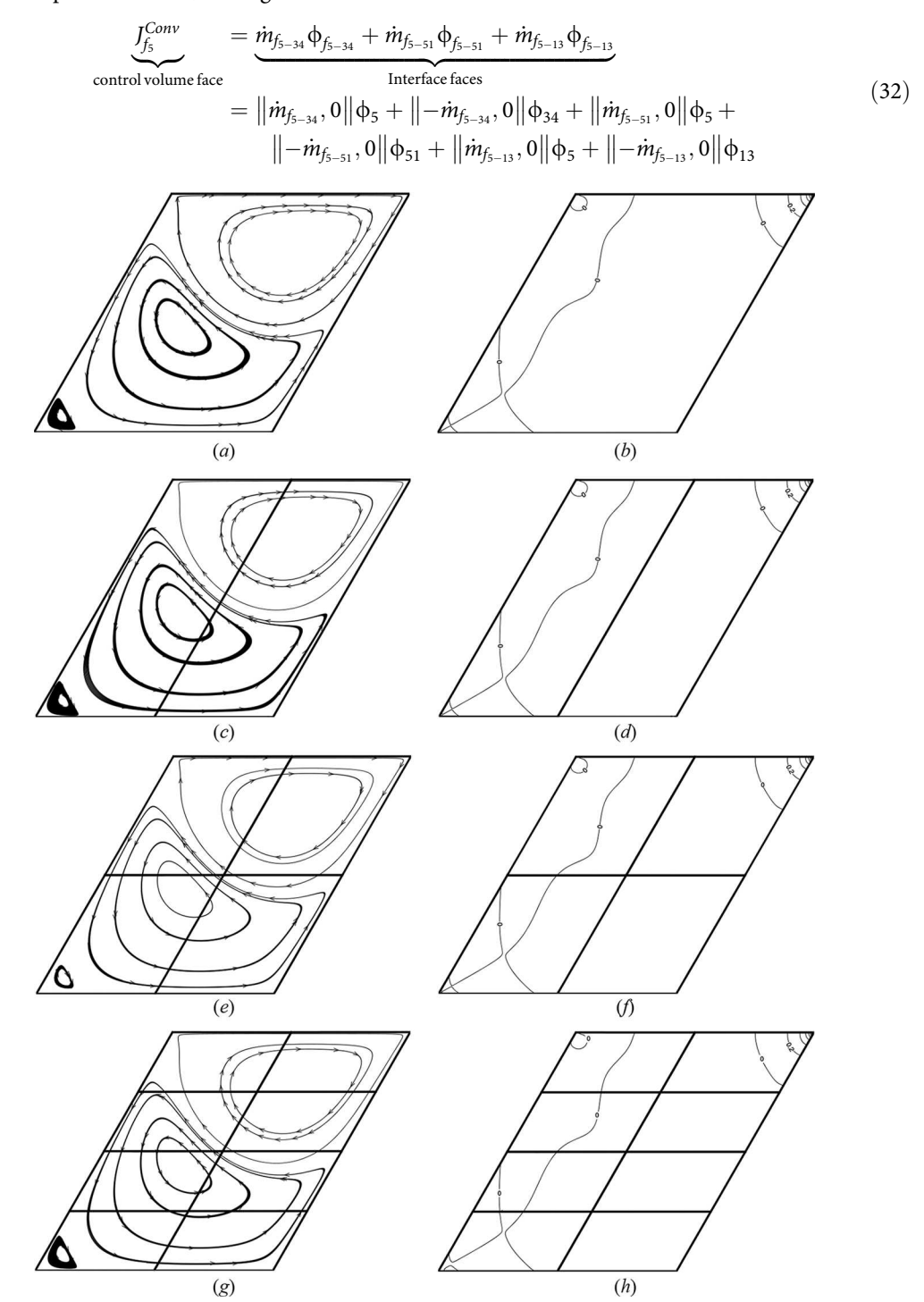


Figure 9. Comparison of (a, c, e, g) streamlines and (b, d, f, h) isobars for the lid-driven flow in a skew cavity problem generated using quadrilateral/hybrid elements with the domain subdivided into (a, b) one, (c, d) two, (e, f) four, and (g, h) eight blocks (segregated solver).

and the general expression of the convection flux when an element i of region 1 is connected to n elements of region 2 is given by

$$J_{f_i}^{\text{Conv}} = \sum_{j=1}^{n} \| \dot{m}_{f_{i-j}}, 0 \| \phi_i + \sum_{j=1}^{n} \| - \dot{m}_{f_{i-j}}, 0 \| \phi_j$$
 (33)

#### Discretization of the diffusion flux

The diffusion flux is computed using

control volume face
$$\frac{\int_{f_{5-34}}^{Diff} \nabla \phi_{f_{5-34}} \cdot S_{f_{5-34}} + \Gamma_{f_{5-31}} \nabla \phi_{f_{5-31}} \cdot S_{f_{5-31}} \cdot S_{f_{5-13}}}{\text{Interface faces}} \\
= \left( \phi_{f_{54}} - \phi_{f_{5}} \right) \frac{E_{f_{5-34}}}{d_{5-34}} + \left( \phi_{f_{51}} - \phi_{f_{5}} \right) \frac{E_{f_{5-31}}}{d_{5-51}} + \left( \phi_{f_{13}} - \phi_{f_{5}} \right) \frac{E_{f_{5-13}}}{d_{5-13}} \\
+ \left[ \Gamma_{f_{5-34}} \nabla \phi_{f_{5-34}} \cdot (S_{f_{5-34}} - E_{f_{5-34}}) + \Gamma_{f_{5-31}} \nabla \phi_{f_{5-31}} \cdot (S_{f_{5-51}} - E_{f_{5-31}}) \right] \\
+ \Gamma_{f_{5-13}} \nabla \phi_{f_{5-13}} \cdot (S_{f_{5-13}} - E_{f_{5-13}}) \\
+ \Gamma_{f_{5-13}} \nabla \phi_{f_{5-13}} \cdot (S_{f_{5-13}} - E_{f_{5-13}}) \\
-0.002 \\
-0.001 \\
-0.002 \\
-0.002 \\
-0.002 \\
-0.002 \\
-0.003 \\
-0.004 \\
-0.004 \\
-0.005 \\
-0.005 \\
-0.005 \\
-0.005 \\
-0.005 \\
-0.005 \\
-0.005 \\
-0.005 \\
-0.005 \\
-0.005 \\
-0.005 \\
-0.005 \\
-0.005 \\
-0.005 \\
-0.005 \\
-0.005 \\
-0.005 \\
-0.005 \\
-0.005 \\
-0.005 \\
-0.005 \\
-0.005 \\
-0.005 \\
-0.005 \\
-0.005 \\
-0.005 \\
-0.005 \\
-0.005 \\
-0.005 \\
-0.005 \\
-0.005 \\
-0.005 \\
-0.005 \\
-0.005 \\
-0.005 \\
-0.005 \\
-0.005 \\
-0.005 \\
-0.005 \\
-0.005 \\
-0.005 \\
-0.005 \\
-0.005 \\
-0.005 \\
-0.005 \\
-0.005 \\
-0.005 \\
-0.005 \\
-0.005 \\
-0.005 \\
-0.005 \\
-0.005 \\
-0.005 \\
-0.005 \\
-0.005 \\
-0.005 \\
-0.005 \\
-0.005 \\
-0.005 \\
-0.005 \\
-0.005 \\
-0.005 \\
-0.005 \\
-0.005 \\
-0.005 \\
-0.005 \\
-0.005 \\
-0.005 \\
-0.005 \\
-0.005 \\
-0.005 \\
-0.005 \\
-0.005 \\
-0.005 \\
-0.005 \\
-0.005 \\
-0.005 \\
-0.005 \\
-0.005 \\
-0.005 \\
-0.005 \\
-0.005 \\
-0.005 \\
-0.005 \\
-0.005 \\
-0.005 \\
-0.005 \\
-0.005 \\
-0.005 \\
-0.005 \\
-0.005 \\
-0.005 \\
-0.005 \\
-0.005 \\
-0.005 \\
-0.005 \\
-0.005 \\
-0.005 \\
-0.005 \\
-0.005 \\
-0.005 \\
-0.005 \\
-0.005 \\
-0.005 \\
-0.005 \\
-0.005 \\
-0.005 \\
-0.005 \\
-0.005 \\
-0.005 \\
-0.005 \\
-0.005 \\
-0.005 \\
-0.005 \\
-0.005 \\
-0.005 \\
-0.005 \\
-0.005 \\
-0.005 \\
-0.005 \\
-0.005 \\
-0.005 \\
-0.005 \\
-0.005 \\
-0.005 \\
-0.005 \\
-0.005 \\
-0.005 \\
-0.005 \\
-0.005 \\
-0.005 \\
-0.005 \\
-0.005 \\
-0.005 \\
-0.005 \\
-0.005 \\
-0.005 \\
-0.005 \\
-0.005 \\
-0.005 \\
-0.005 \\
-0.005 \\
-0.005 \\
-0.005 \\
-0.005 \\
-0.005 \\
-0.005 \\
-0.005 \\
-0.005 \\
-0.005 \\
-0.005 \\
-0.005 \\
-0.005$$

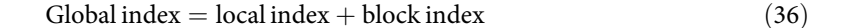
**Figure 10.** Comparison of pressure, *u*-velocity, and *v*-velocity profiles along the horizontal centerline of the cavity generated using quadrilateral/hybrid elements with the domain subdivided into one, two, four, and eight blocks (segregated solver).

with the general expression given by

$$J_{f_{i}}^{Diff} = \sum_{j=1}^{n} \left( \phi_{f_{j}} - \phi_{f_{i}} \right) \frac{E_{f_{i-j}}}{d_{i-j}} + \underbrace{\sum_{j=1}^{n} \Gamma_{f_{i-j}} \nabla \phi_{f_{i-j}} \cdot \left( \mathbf{S}_{f_{i-j}} - \mathbf{E}_{f_{i-j}} \right)}_{\text{Non-orthogonal terms}}$$
(35)

where  $\mathbf{E}_{f_{i-i}}$  is in the direction of the line connecting the points *i* and *j*.

Since the discretization now involves elements from different blocks, local element numbering can no longer be used. To this end, a global element index is defined to ensure that the assembly across regions is congregated properly into the global matrix of coefficients. The global index is computed following a simple mapping procedure. The procedure starts with indexing blocks (or regions) and associating with each a number representing the sum of elements that are in all blocks (or regions) of lower index. The global element index is obtained by adding to the local element index, the block (or region) index. This ensures that the positions of the coefficients for each element are unique and easily obtained from local block (or region) information. Mathematically the reindexing equation is given by



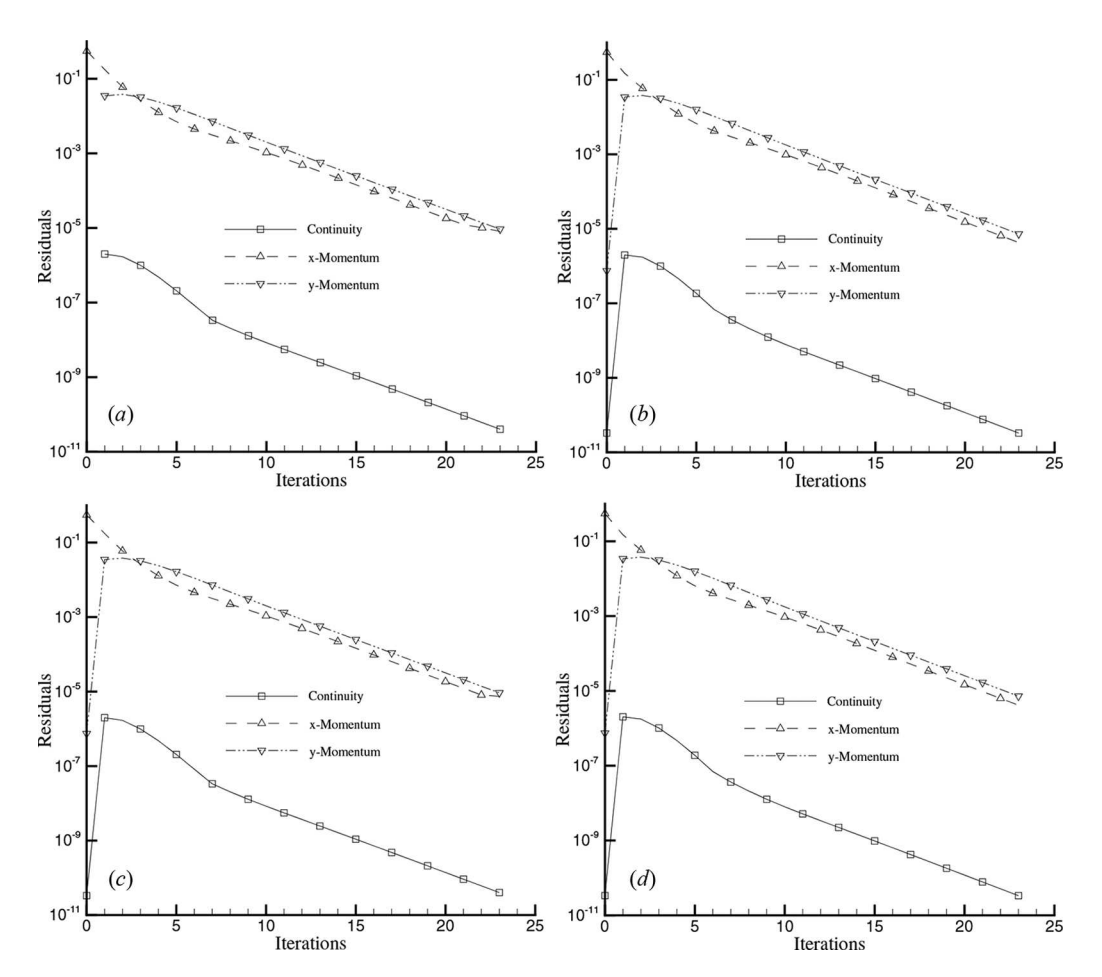


Figure 11. Reduction of residuals with iterations for the flow in a skew cavity using triangular elements and the coupled flow solver with the domain subdivided into (a) one block, (b) two blocks, (c) four blocks, and (d) eight blocks.



#### **Results and discussion**

The performance of the multiblock coupling algorithm is evaluated by solving the following three incompressible laminar flow problems: (i) lid-driven flow in a skew cavity, (ii) flow behind a backward facing step, and (iii) sudden expansion in a rectangular cavity. Results to problems are

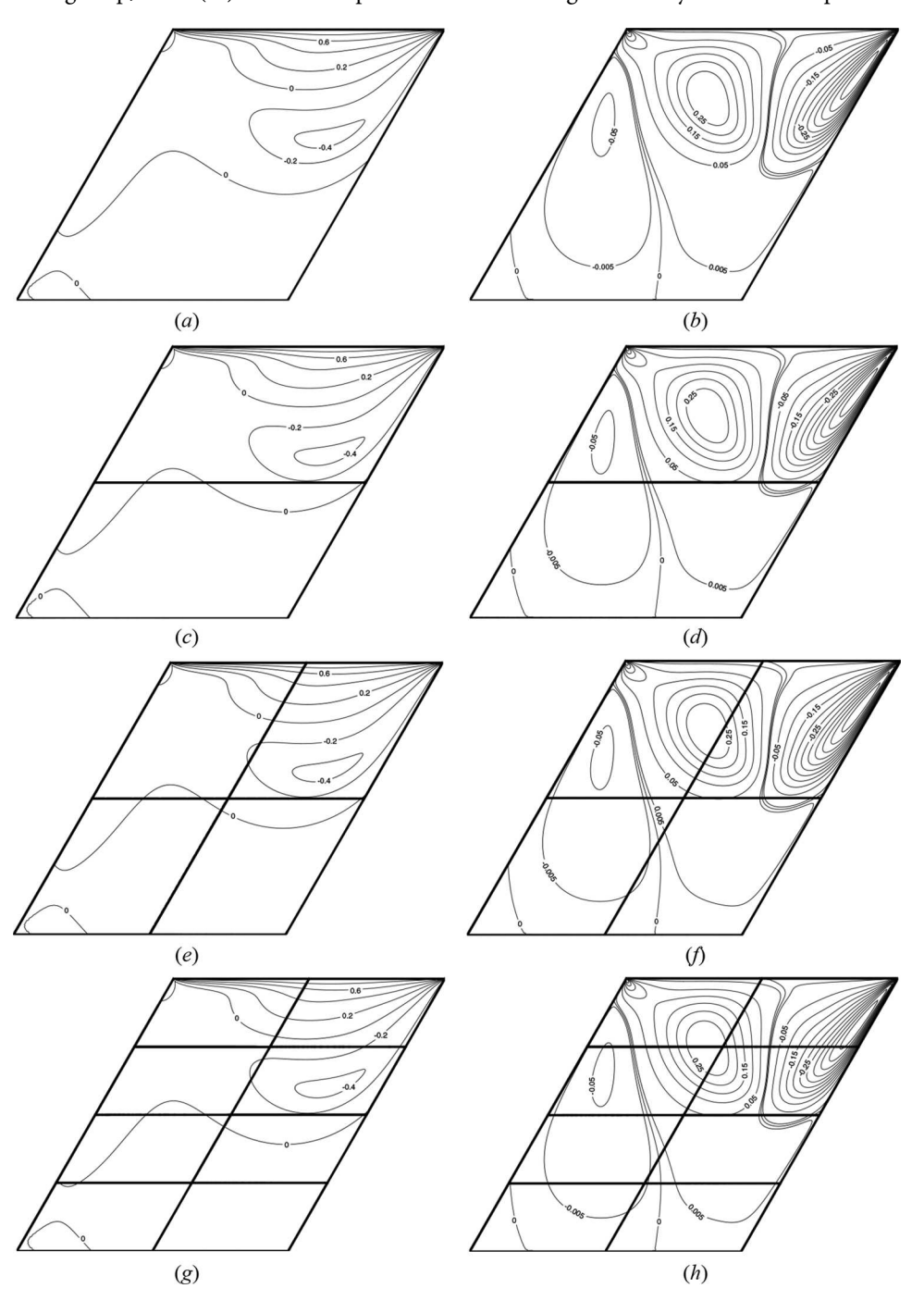


Figure 12. Comparison of (a, c, e, g) u-velocity and (b, d, f, h) v-velocity contours for the lid-driven flow in a skew cavity problem generated using triangular elements with the domain subdivided into (a, b) one, (c, d) two, (e, f) four, and (g, h) eight blocks (coupled solver).

computed using triangular, quadrilateral, and/or hybrid (i.e., a combination of triangular and quadrilateral) elements. The neighboring blocks in a multiblock configuration are meshed with a slight difference in the mesh density to ensure that grids are nonmatching at the interface, while maintaining almost the same total number of elements as for the single-block mesh. Moreover, all problems are solved with the segregated solver over a single block and multiblocks, with limited computations reported for the coupled solver. When solving the same problem with different number of blocks, the same initial guess is used. For all test cases, computations were stopped when the maximum residual of all variables drops below a vanishing quantity that was set at  $10^{-5}$ . Under relaxation was required with the segregated solver. The under-relaxation factors were set at 0.7 and 0.3 for the momentum and continuity equation, respectively. The efficiency of the proposed multiblock solver is demonstrated by comparing the number of iterations to convergence required by each meshing technique.

#### Problem 1: Lid-driven flow in a skew cavity

The first problem is a well-known Computational Fluid Dynamics (CFD) test case that has been used by several workers as a benchmark [41]. A schematic of the physical situation is depicted in Figure 7 (a) and represents a skew cavity with horizontal sides of length L and the distance between the lower and upper horizontal sides L. The side walls of the cavity are skewed at an angle of 60° with respect to the horizontal side. The nonmatching interface grids are displayed in Figure 7(b)-7(d) for quadrilateral, triangular, and hybrid elements, respectively. The domain is subdivided into one, two, four, or eight blocks and results are presented for a value of Reynolds number ( $Re = \rho UL/\mu$ , where U is the velocity of the top horizontal wall and is set to 1) of 765. Results are generated using the segregated solver with quadrilateral and hybrid elements and the coupled solver with triangular elements.

The convergence history plots showing the reduction in the maximum residuals of the momentum and continuity equations with the segregated solver are displayed in Figure 8(a)-8(d) for the cases when the domain is subdivided into one, two, four, and eight blocks, respectively. As shown, the convergence behavior for all cases is similar with the total number of iterations to reach convergence, displayed in Table 1, varying between 2,365 and 2,379. Given the slight variation in the number of elements, this clearly shows that the convergence rate is unaffected by the number of blocks into which the domain is subdivided. The solution independence of the number of blocks used is demonstrated by the streamlines and isobars presented in Figure 9. Results for the cases when the domain is subdivided into one [Figure 9(a) and 9(b)], two [Figure 9(c) and 9(d)], and eight [Figure 9(g) and 9(h)] blocks are obtained using quadrilateral elements, while for the case when

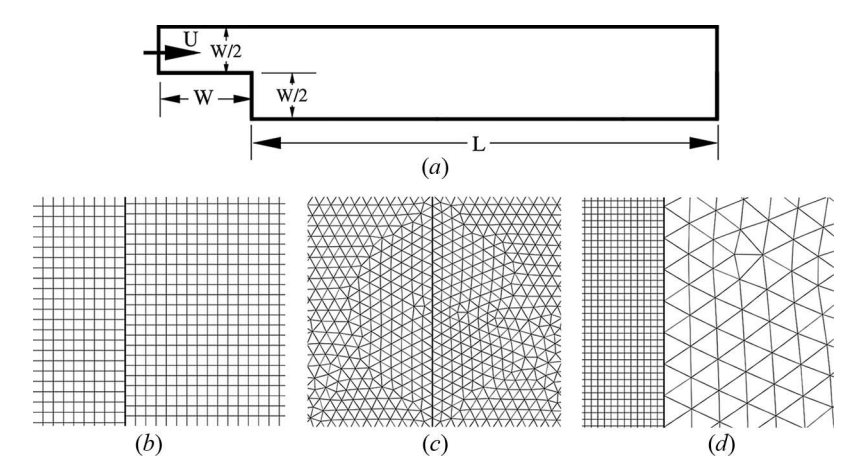


Figure 13. (a) Physical domain for the flow behind a backward facing step; nonmatching grids at the interface between two blocks using (b) quadrilateral, (c) triangular, and (d) hybrid elements.

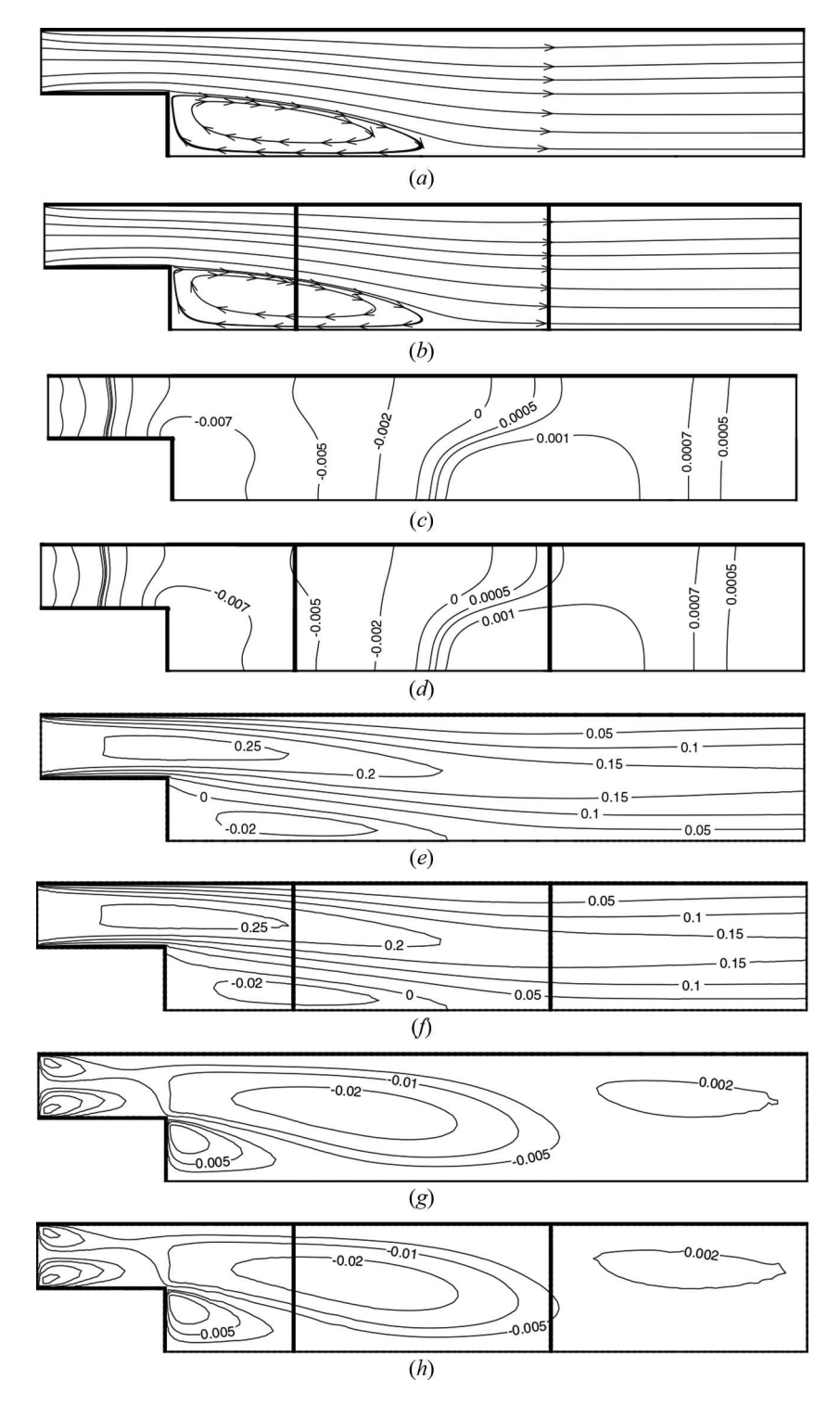


Figure 14. Comparison of (a, b) streamlines, (c, d) isobars, (e, f) u-velocity contours, and (g, h) v-velocity contours for the flow behind a backward facing step generated by subdividing the domain into one (a, c, e, g) and three (b, d, f, h) blocks.

the domain is subdivided into four blocks [Figure 9(e) and 9(f)], results are obtained with hybrid elements. As shown, streamlines and isobars are similar, indicating that solutions are independent of the number of blocks and the type of elements used. This is further confirmed by the pressure, u-velocity, and v-velocity profiles presented in Figure 10(a)-10(c), respectively. As shown, profiles are on top of each other demonstrating the correctness of the newly developed treatment along nonmatching grid interfaces.

The physical domain depicted in Figure 7(a) is again decomposed into one, two, four, and eight blocks, meshed using triangular elements, and solutions for the flow field within the domain are generated using the coupled flow solver.

The residual history plots displayed in Figure 11(a)-11(d) and few iterations needed for convergence reported in Table 1 demonstrate that the rate of convergence is independent of few connected regions (in all cases, 23 iterations are needed), which is a clear indication of a strong implicit interface coupling and that the coupling technique is implemented efficiently with minimum overhead on memory and computational resources. Moreover, the u-velocity and v-velocity contours presented in Figure 12 indicate that the solution obtained by decomposing the domain into 2 [Figure 12(c) and 12(d)], 4 [Figure 12(e) and 12(f)], or 8 [Figure 12(g) and 12(h)] regions is exactly the one resulting from solving the problem as one block [Figure 12(a) and 12(b)]. Furthermore, the continuity of contours at interfaces clearly indicates that fluxes across interfaces are fully conserved.

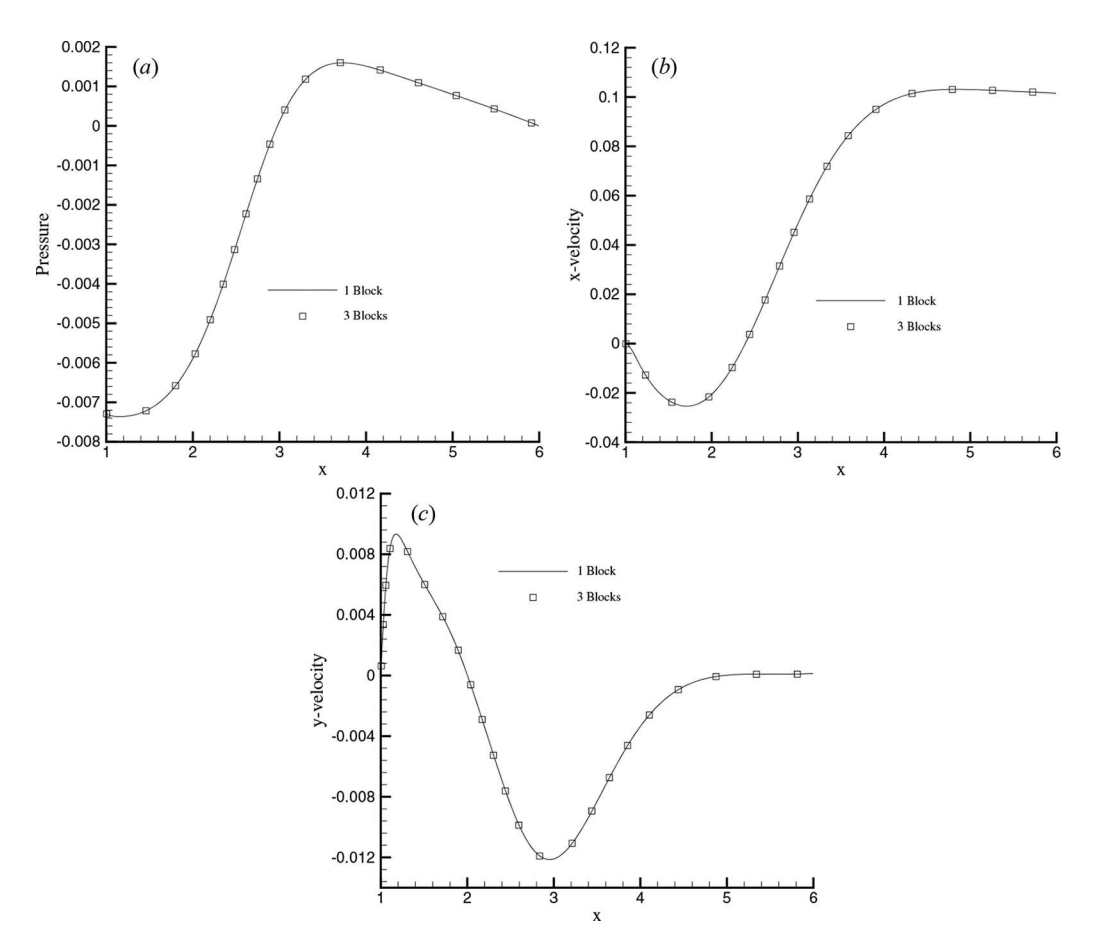
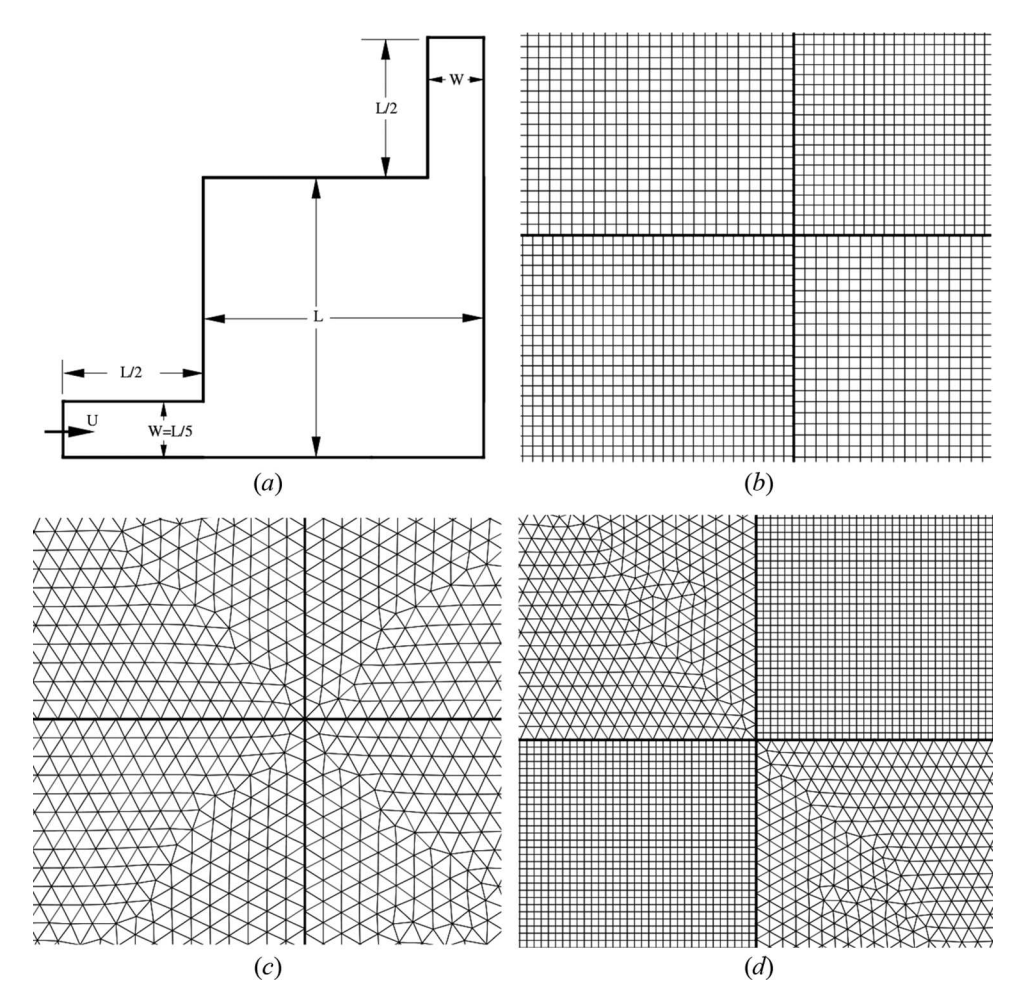


Figure 15. Comparison of (a) pressure, (b) x-velocity, and (c) y-velocity profiles along the horizontal centerline of the cavity generated with the domain subdivided into one and three blocks.

#### Problem 2: Flow behind a backward facing step

The physical domain for the problem is displayed in Figure 13(a) and represents the flow of a fluid over a backward facing step. It is used here to show the performance of the coupling technique in predicting the separation and reattachment points. The problem is solved for an expansion ratio of 2. The length and height of the inlet section upstream of the step are W and W/2, respectively. On the other hand, the length L of the section downstream of the step is 5W and its height is W. The flow velocity at the inlet is set to 1. Schematics of the various nonmatching interface grid types are displayed in Figure 13(b)-13(d) for quadrilateral, triangular, and hybrid elements, respectively.

Solutions for the problem are generated for the cases when the domain is either treated as one block or subdivided into three blocks. The numbers of iterations required for convergence are presented in Table 1. For a given grid type, the convergence behavior (not presented for compactness) and the number of iterations required to get a converged solution are independent of the number of blocks used. For a grid composed of 55,000 quadrilateral elements, the number of iterations required is 2,251 for one block and 2,244 for three blocks. These numbers are, respectively, 626 and 632 for a grid composed of a little over 5,000 triangular elements. The one-block and three-block results generated using the dense quadrilateral grid system are displayed in the form of streamlines, isobars, u-velocity contours, and v-velocity contours in Figure 14(a)-14(h). As shown, one-block and



**Figure 16.** (a) Physical domain for the flow due to sudden expansion in a square cavity; Nonmatching grids at the interfaces using (b) quadrilateral, (c) triangular, and (d) hybrid elements.

three-block results are identical with interface fluxes being conserved as demonstrated by the continuity of the contour plots at interfaces. This is further revealed by the pressure, u-velocity, and v-velocity profiles along the horizontal line y = W/2 (i.e., along mid-height of the domain after the step, 1 < x < 6) presented in Figure 15(a)–15(c), respectively. As shown, results are on top of each other confirming again the correctness of the suggested treatment at nonmatching grid interfaces.

#### Problem 3: Sudden expansion in a square cavity

The last problem considered in this paper deals with the sudden expansion of a steady, laminar, and two-dimensional flow entering a square cavity of side L. The physical configuration is schematically depicted in Figure 16(a). As shown, the inlet and outlet to the domain are rectangular sections of length

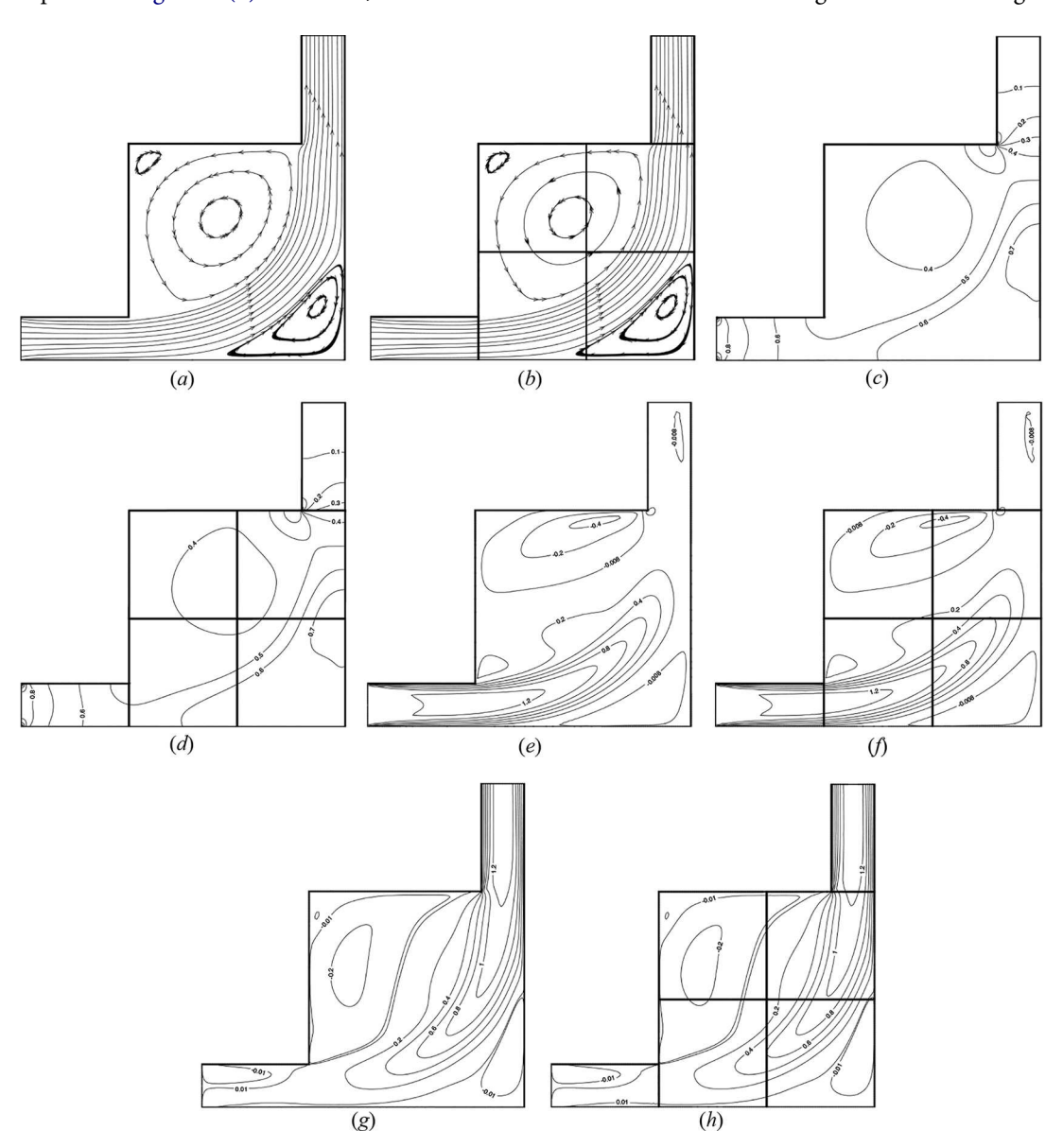
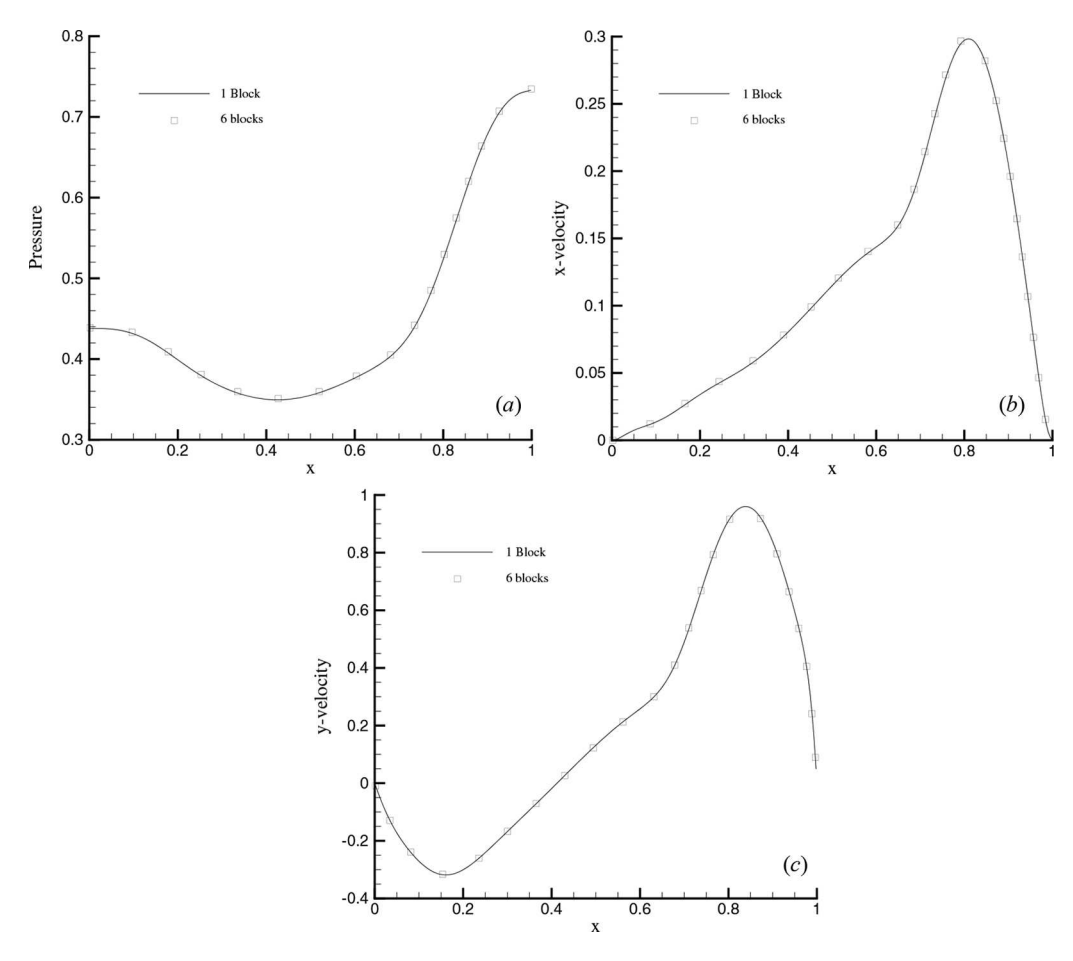


Figure 17. Comparison of (a, b) streamlines, (c, d) isobars, (e, f) u-velocity contours, and (g, h) v-velocity contours for the flow behind a backward facing step generated by subdividing the domain into one (a, c, e, g) and six (b, d, f, h) blocks.



**Figure 18.** Comparison of pressure, *u*-velocity, and *v*-velocity profiles along the horizontal centerline of the cavity generated using quadrilateral/hybrid elements with the domain subdivided into one and six blocks.

L/2 and of width W = L/5. The quadrilateral, triangular, and hybrid nonmatching interface grid types are displayed in Figure 16(b)-16(d), respectively. The u-velocity at inlet is set to 1. Solutions for the problem are computed with grid generated either by considering the domain as one block or by subdividing it into six blocks and independently generating grids that are nonmatching at interfaces.

As reported in Table 1, the numbers of iterations required for convergence are independent of the number of blocks used. For a grid composed of 48,000 quadrilateral elements, the number of iterations needed is 1,909 for one block and 1,920 for six blocks. These numbers are, respectively, 2,304 and 2,273 for a grid composed of nearly 27,000 triangular elements. Streamlines, isobars, u-velocity contours, and v-velocity contours generated using triangular grids are displayed in Figure 17(a)-17(h). Once more, the one-block and six-block results are identical with full conservation of fluxes at interfaces as can be inferred from the continuity of the contour plots presented. Another confirmation of results is shown in Figure 18, where pressure [Figure 18(a)], u-velocity [Figure 18(b)], and v-velocity [Figure 18(c)] profiles along the horizontal centerline of the square cavity generated using one block and six blocks fall on top of each other.

#### Closing remarks

A fully implicit multiblock mesh coupling technique preserving the convergence characteristics of single-block meshing was presented. The scheme was developed in the context of the finite volume



method and was shown to be applicable to pressure-based segregated and coupled solvers. The test problems demonstrated that the method results in a strong implicit interface coupling and is efficient with its convergence rate independent of the number of connected regions, conserves interface fluxes, and allows the discretization of the various regions to be performed independently.

#### **Funding**

The financial support provided by the University Research Board of the American University of Beirut is gratefully acknowledged.

#### References

- [1] D. You, R. Mittal, M. Wang, and P. Moin, Large-Eddy Simulation of a Rotor Tip-clearance Flow, AIAA Paper 2002-0981, 2002.
- [2] R. Mittal, S. Venkatasubramanian, and F. M. Najjar, Large Eddy Simulation of Flow through a Low-Pressure Turbine, AIAA Paper 2001-2560, 2001.
- [3] M. Wang and P. Moin, Computation of Trailing-edge Flow and Noise Using Large-Eddy Simulation, AIAA J., vol. 38, pp. 2201-2209, 2000.
- [4] C. Erath and D. Praetorius, A Posteriori Error Estimate and Adaptive Mesh Refinement for the Cell-centered Finite Volume Method for Elliptic Boundary Value Problems, SIAM J. Numer. Anal., vol. 47, no. 1, pp. 109–135, 2008.
- [5] M. A. Martins, R. M. Valle, L. S. Oliveira, and D. Burgarelli, Error Estimation and Adaptivity for Finite Volume Methods on Unstructured Triangular Meshes: Elliptic Heat Transfer Problems, Numer. Heat Transfer Part B Fundam., vol. 42, pp. 461-483, 2002.
- [6] A. Rouboa and E. Monteiro, Heat Transfer in Multi-block Grid During Solidification: Performance of Finite Differences and Finite Volume Methods, J. Mater. Process. Technol., vol. 204, pp. 451-458, 2008.
- [7] Y. Guowei, K. Masahiro, and O. Shigeru, Multiblock Navier-Stokes Solver for Wing/Fuselage Transport Aircraft, JSME Int. J. Ser. B Fluids Therm. Eng., vol. 45, no. 1, pp. 85-90, 2002.
- [8] C. W. Lin, G. D. Smith, and S. C. Fisher, Application of a Multiblock Grid Generation Approach to Ship Configuration, 3rd International Conference on Numerical Grid Generation in CFD, Spain, June 1991.
- [9] R. L. Meakin, Composite Overset Structured Grids, in Thompson, Soni, and Weatherill (eds.), Handbook of Grid Generation, chap. 11, CRC Press, 1999.
- [10] Y. Zheng and M. S. Liou, A Novel Approach of Three-dimensional Hybrid Grid Methodology: Part 1. Grid Generation, Comput. Methods Appl. Mech. Eng., vol. 192, pp. 4147-4171, 2003.
- [11] L. Saas, I. Faille, F. Nataf, and F. Willien, Finite Volume Methods for Domain Decomposition on Non-matching Grids with Arbitrary Interface Conditions, SIAM J. Numer. Anal., vol. 43, no. 2, pp. 860-890, 2005.
- [12] R. Eymard and R. Herbin, A New Collocated Finite Volume Scheme for the Incompressible Navier-Stokes Equations on General Non Matching Grids, C. R. Acad. Sci. Ser. I Math., vol. 344, pp. 659-662, 2007.
- [13] E. Aulisa, S. Manservisi, and P. Seshaiyer, A Computational Multilevel Approach for Solving 2D Navier-Stokes Equations over Non-matching Grids, Comput. Methods Appl. Mech. Eng., vol. 195, pp. 4604-4616, 2006.
- [14] O. Steinbach, A Natural Domain Decomposition Method with Non-matching Grids, Appl. Numer. Math., vol. 54, pp. 362-377, 2005.
- [15] L. Chang and G. Yuan, Cell-centered Finite Volume Methods with Flexible Stencils for Diffusion Equations on General Nonconforming Meshes, Comput. Methods Appl. Mech. Eng., vol. 198, pp. 1638-1646, 2009.
- [16] Z. Lilek, S. Muzaferija, M. Peric, and V. Seidl, An Implicit Finite Volume Method Using Non-matching Blocks of Structured Grid, Numer. Heat Transfer Part B Fundam., vol. 32, no. 4, pp. 385-401, 1997.
- [17] C. Romé and S. Glockner, An Implicit Multiblock Coupling for the Incompressible Navier-Stokes Equations, Int. J. Numer. Methods Fluids, vol. 47, pp. 1261-1267, 2005.
- [18] A. Pantano and R. C. Averill, A Penalty-based Interface Technology for Coupling Independently Modeled 3D Finite Element Meshes, Finite Elem. Anal. Des., vol. 43, pp. 271-286, 2007.
- [19] A. D. de Boer, A. H. van Zuijlen, and H. Bijl, Review of Coupling Methods for Non-matching Meshes, Comput. Methods Appl. Mech. Eng., vol. 196, pp. 1515–1525, 2007.
- [20] M. J. Smith, C. E. S. Cesnik, and D. H. Hodges, Evaluation of Some Data Transfer Algorithms for Noncontiguous Meshes, J. Aerosp. Eng., vol. 13, no. 2, pp. 52-58, 2000.
- [21] M. Darbandi and A. Naderi, Multiblok Hybrid Grid Finite Volume Method to Solve Flow in Irregular Geometries, Comput. Methods Appl. Mech. Eng., vol. 196, pp. 321-336, 2006.
- [22] S. V. Patankar, A Calculation Procedure for Two Dimensional Elliptic Situations, Numer. Heat Transfer, vol. 4,
- [23] S. V. Patankar, Numerical Heat Transfer and Fluid Flow, Hemisphere, NY, 1980.



- [24] S. V. Patankar, and D. B. Spalding, A Calculation Procedure for Heat, Mass and Momentum Transfer in Three-dimensional Parabolic Flows, Int. J. Heat Mass Transfer, vol. 15, no. 10, pp. 1787-1806, 1972.
- [25] M. Darwish, D. Asmar, and F. Moukalled, A Comparative Assessment within a Multigrid Environment of Segregated Pressure-based Algorithms for Fluid Flow at all Speeds, Numer. Heat Transfer Part B Fundam., vol. 45, pp. 49-74, 2004.
- [26] F. Moukalled and M. Darwish, A High-resolution Pressure-based Algorithm for Fluid Flow at All Speeds, J. Comput. Phys., vol. 168, no.1, pp. 101–133, 2001.
- [27] F. Moukalled and M. Darwish, A Unified Formulation of the Segregated Class of Algorithms for Fluid Flow at All Speeds, Numer. Heat Transfer Part B Fundam., vol. 37, no 1, pp. 103-139, 2000.
- [28] F. Moukalled, L. Mangani, and M. Darwish, The Finite Volume Method in Computational Fluid Dynamics: An Advanced Introduction with OpenFOAM® and Matlab®, Springer International Publishing, Switzerland, 2015.
- [29] F. Moukalled and M. Darwish, Pressure Based Algorithms for Single and Multifluid Flows, in W. J. Minkowycz E. M. Sparrow, and J. Y. Murthy (eds.), Handbook of Numerical Heat Transfer, 2nd ed., pp. 325-367, Wiley, 2006.
- [30] C. M. Rhie and W. L. Chow, Numerical Study of The Turbulent Flow Past An Airfoil with Trailing Edge Separation, AIAA J., vol. 21, pp. 1525–1532, 1983.
- [31] A. Carmona, O. Lehmkuhl, C. D. Perez-Segarra, and A. Oliva, Numerical Analysis of the Transpose Diffusive Term for Viscoplastic-type Non-Newtonian Fluid Flows using a Collocated Variable Arrangement, Numer. Heat Transfer Part B Fundam., vol. 67, no. 5, pp. 410-436, 2015.
- [32] P. Roy, N. K. Anand, and D. Donzis, A Parallel Multigrid Finite-volume Solver on a Collocated Grid for Incompressible Navier-Stokes Equations, Numer. Heat Transfer Part B Fundam., vol. 67, no. 5, pp. 376-409, 2015.
- [33] D. K. Kolmogorov, W. Z. Shen, N. N. Sorensen, and J. N. Sorensen, Fully Consistent Simple-like Algorithms on Collocated Grids, Numer. Heat Transfer Part B Fundam., vol. 67, no. 2, pp. 101-123, 2015.
- [34] F. Wang, W. Zhang, and Y. Li, Fourrier Analysis of the Effect of Momentum Interpolation on the SIMPLE Series Formulated on a Collocated Grid, Numer. Heat Transfer Part B Fundam., vol. 64, no. 1, pp. 48-70, 2013.
- [35] L. Bu, J. Zhao, and K. J. Tseng, Study on Momentum Interpolation Methods with Curvilinear Collocated Grids in Single-phase and Two-phase Flows, Numer. Heat Transfer Part B Fundam., vol. 61, no. 4, pp. 298-310, 2012.
- [36] M. Darwish, A. Abdel Aziz, and F. Moukalled, A Coupled Pressure-based Finite Volume Solver for Incompressible Two-phase Flow, Numer. Heat Transfer Part B Fundam., vol. 67, no. 1, pp. 47-74, 2015.
- [37] M. Darwish and F. Moukalled, A Fully Coupled Navier-Stokes Solver for Fluid Flow at All Speeds," Numer. Heat Transfer Part B Fundam., vol. 45, pp. 410-444, 2014.
- [38] F. Moukalled, A. Abdel Aziz, and M. Darwish, Performance Comparison of the NWF and DC Methods for Implementing High-resolution Schemes in a Fully Coupled Incompressible Flow Solver, Appl. Math. Comput., vol. 217, no. 11, pp. 5041-5054, 2011.
- [39] M. Darwish, I. Sraj, and F. Moukalled, A Coupled Finite Volume Solver for the Solution of Incompressible Flows on Unstructured Grids, J. Comput. Phys., vol. 28, no. 1, pp. 180–201, 2009.
- [40] M. Darwish, I. Sraj, and F. Moukalled, A Coupled Incompressible Flow Solver on Structured Grids, Numer. Heat Transfer Part B Fundam., vol. 52, pp. 353-371, 2007.
- [41] F. Moukalled, and M. Darwish, New Bounded Skew Central Difference Scheme, Part I: Formulation and Testing, Numer. Heat Transfer, Part B Fundam., vol. 31, pp. 91–110, 1997.